Dinuclear Design of a Pt(II) Complex Affording Highly Efficient Red Emission: Photophysical Properties and Application in Solution-Processible OLEDs

Marsel Z. Shafikov,*[,†,¥,‖] Ruth Daniels,[‡] Piotr Pander,[¶] Fernando B. Dias,[¶] J. A. Gareth Williams*[,§] and Valery N. Kozhevnikov*[,‡]

† *Institut für Physikalische und Theoretische Chemie, Universität Regensburg, Universitätsstrasse 31, Regensburg, D-93053, Germany. E-mail: shafikoff@gmail.com*

¥ *Ural Federal University, Mira 19, Ekaterinburg, 620002, Russia.*

‖ *Department of Chemistry, University of York, Heslington, York, YO10 5DD, U.K.*

‡ *Department of Applied Sciences, Northumbria University, Newcastle upon Tyne, NE1 8ST, U.K. E-mail: valery.kozhevnikov@northumbria.ac.uk*

¶ *Department of Physics, Durham University, Durham, DH1 3LE U.K.*

§ *Department of Chemistry, Durham University, Durham, DH1 3LE U.K. E-mail: j.a.g.williams@durham.ac.uk*

ABSTRACT

The light-emitting efficiency of luminescent materials is invariably compromised on moving to the red and near infrared regions of the spectrum, due to the transfer of electronic excited state energy into vibrations. We describe how this undesirable "energy gap law" can be side-stepped for phosphorescent organometallic emitters through the design of a molecular emitter that incorporates two platinum(II) centres. The dinuclear cyclometallated complex of a substituted 4,6-bis(2-thienyl)pyrimidine emits very brightly in the red region of the spectrum (λ_{max} = 610 nm, Φ = 0.85 in deoxygenated CH_2Cl_2 at 300 K). The lowest-energy absorption band is extraordinarily intense for a cyclometallated metal complex: at λ = 500 nm, ε = 53800 M^{-1} cm^{-1}. The very high efficiency of emission achieved can be traced to an unusually high rate constant for the $T_1 \rightarrow S_0$ phosphorescence process, allowing it to compete effectively with non-radiative vibrational decay. The high radiative rate constant correlates with an unusually large zero-field splitting of the triplet state, which is estimated to be 40 cm^{-1} by means of variable-temperature time-resolved spectroscopy over the range $1.7 < T < 120$ K. The compound has been successfully tested as a red phosphor in an organic light-emitting diode (OLED) prepared by solution processing. The results highlight a potentially attractive way to develop highly efficient red and NIR-emitting devices through the use of multinuclear complexes.

KEYWORDS

Electroluminescence; near-infrared emission; deep-red luminescence; triplet harvesting; dinuclear platinum complex.

INTRODUCTION

Phosphorescent metal complexes continue to attract huge interest as emitting materials for organic light-emitting diodes (OLEDs) due to the high emission efficiencies that they may offer.[1,2,3,4] High spin-orbit-coupling (SOC) associated with the metal ion promotes emission from the otherwise wasted triplet states – formed upon charge recombination in a device in ratios of up to 3:1 relative to singlets.[5] Phosphorescent iridium complexes are now routinely used as green and orange/red emitters in many mass-produced consumer devices. Other strategies for increasing efficiency have also emerged recently, such as the use of E-type or thermally activated delayed fluorescence (TADF), whereby a small S_1–T_1 energy gap allows repopulation of the emissive singlet state from a normally non-emissive triplet.[6,7,8] Although purely organic molecules can then be used, triplet-emitting metal complexes remain attractive, particularly in terms of stability (to favour long device lifetime) and the ability to tune emission wavelengths through rational structural modification. Meanwhile, such molecular metal complexes are proving to be of interest in other areas where intense emission is required, for example, as probes suitable for time-resolved detection in bio-imaging and sensing.[9,10,11,12]

The vast majority of complexes explored to date are mononuclear, *i.e.,* they feature one metal ion per molecule. However, multinuclear metal complexes – featuring two or more metal ions linked via rigid bridging ligands – have begun to emerge as a distinct class of phosphorescent molecules.[13,14] In particular, dinuclear Ir(III) and Pt(II) complexes bridged by cyclometallating, pyrimidine-based ligands display unusually high phosphorescence quantum yields, apparently due to unusually high triplet radiative decay rate constants k_r.[15,16,17,18,19] This property of enhanced k_r is especially attractive for the development of deeply red-emitting systems, since the efficiencies of visible emitters normally fall off at long wavelengths. The non-radiative decay of electronic excited states increases as the energy gap decreases, since coupling with higher vibrational levels of the ground state is facilitated – the so-called *energy gap law*.[20] Since the photoluminescence quantum yield depends on the relative magnitudes of

the radiative k_r and non-radiative Σk_{nr} decay rate constants, it is clear that systems with enhanced k_r are essential if efficient deep red emitters are to be obtained.[21] Ironically, in mononuclear complexes, k_r typically falls off for red phosphors, because the strategy for red-shifting normally involves increasing conjugation within the ligand, which is accompanied by a decrease in metal character in the excited state and hence by a decrease in the efficiency of SOC.[22,23]

Despite growing experimental evidence that multinuclearity increases the rate of spin-forbidden transitions ($S_n \rightarrow T_n$ intersystem crossing and $T_1 \rightarrow S_0$ phosphorescence), very few studies have sought to probe the origins of this effect, by coupling detailed spectroscopy with computational work for instance. Moreover, in terms of device testing, OLEDs that incorporate multinuclear complexes have been largely limited to iridium systems,[24] and only a few isolated examples of OLEDs with polynuclear Pt(II) complexes have been demonstrated.[25,26,27]

In this contribution, we describe the synthesis, photophysical and electrochemical properties of the new dinuclear complex $Pt_2L(acac)_2$ (Figure 1). A detailed examination of the emission properties at cryogenic temperatures (T down to 1.7 K) has been carried out in order to shed light on the influence of the second metal ion on the SOC process. These results are interpreted with the aid of calculations employing time-dependent density functional theory (TD-DFT). A preliminary evaluation of the complex as a phosphorescent red dopant in a solution-processed OLED is also made.

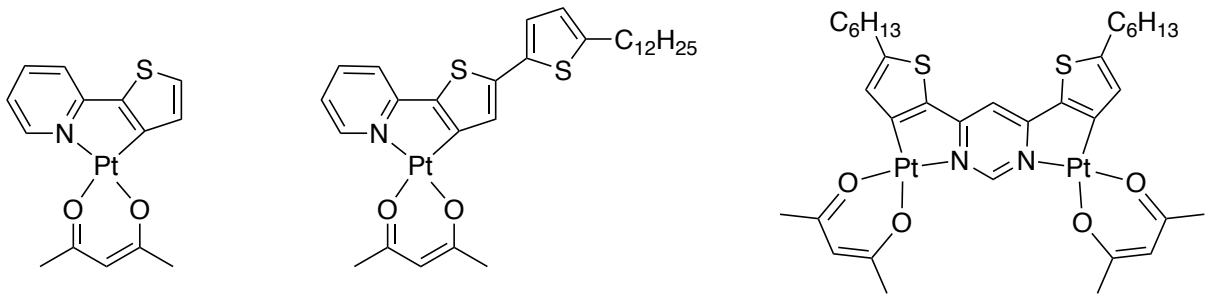

Figure 1 *The structure of the new dinuclear Pt(II) complex $Pt_2L(acac)_2$ studied in this work, together with related mononuclear complexes incorporating thienylpyridine ligands.*

RESULTS AND DISCUSSION

(i) Strategy and choice of target molecule

The most successful and most widely investigated phosphorescent metal complexes are those based on *C^N*-cyclometallating aryl-heterocycle ligands, of which 2-phenylpyridine (ppy) is the archetypal example.[28,29,30,31,32] For example, *fac*-$Ir(ppy)_3$ is one of the most brightly luminescent metal complexes known,[33,34] whilst Pt(ppy)(*O^O*) and Pt(ppy)(*N^O*) complexes are also strongly luminescent (where *O^O* and *N^O* represent bidentate anionic ligands such as acac or picolinate and their derivatives respectively).[35] Such complexes of ppy generally emit in the green region of the spectrum. The emissive excited state is typically formulated as $^3[d_M/\pi_{ppy} \rightarrow \pi^*_{ppy}]$ (or mixed ^{3}LLCT/MLCT), with the participation of the metal in the HOMO ensuring an element of SOC to promote the formally forbidden phosphorescence process.[36,37,38,39,40]

In targeting red emission, a common strategy has been to use *C^N* ligands that incorporate more electron-rich aryl groups, such as thiophene and benzothiophene.[41,42,43,44,45] They serve to raise the HOMO energy, thus lowering the HOMO–LUMO gap and red-shifting emission, but this effect comes

at the expense of metal participation in the excited state, and k_r values are reduced. Previously, we studied the complex Pt(thpy)(acac) (Figure 1) and derivatives carrying one or two 2-thienyl substituents in the 5-position of the thiophene ring.[22] Pt(thpy)(acac) is an orange emitter with k_r = 1.7×10^4 s^{-1}, as compared to a higher value of 5.8×10^4 s^{-1} for the green-emitting Pt(ppy)(acac). In the current work, we chose to target $Pt_2L(acac)_2$ as a dinuclear analogue of Pt(thpy)(acac), in order to explore whether a red-shift could be achieved relative to the ppy complex *without* compromising k_r. The hexyl substituents were included in order to promote the solubility of the complex, which would otherwise be disfavoured by the extended planar core.

(ii) Synthesis

The target complex can be prepared readily in few steps and in high yield. The requisite ditopic bis-bidentate proligand H_2L was synthesised in 84% yield by a palladium-catalysed Suzuki cross-coupling of 4,6-dichloropyrimidine with the pinacol ester of 5-hexyl-2-thiopheneboronic acid (Scheme 1a). Upon treatment of the proligand with $PtCl_2(NCPh)_2$ or K_2PtCl_4 (2.2 equiv.) in refluxing acetic acid (conditions frequently used for cycloplatination reactions), a highly insoluble precipitate was obtained. The low solubility prevented the unambiguous identification of this material. Based on the fact that *N^C*-cyclometallating ligands like 2-phenylpyridine and 2-thienylpyridine invariably give chloro-bridged dimers of the form $[Pt(N^C)(\mu\text{-}Cl)]_2$ under such conditions,[35] coupled with the unambiguous identification of the products subsequently obtained from this material, an oligomeric formulation $[Pt_2L(\mu\text{-}Cl)_2]_n$ as represented in Scheme 1b seems most likely. Refluxing this material briefly in dimethylsulfoxide led to its solubilisation through cleavage of the chloro bridges, with DMSO acting as a neutral, S-bound ligand, as exploited in our earlier work with mononuclear Pt(II) and Ir(III) complexes.[46,47] The DMSO complex $Pt_2LCl_2(dmso)_2$ was isolated as a deep red solid by precipitation; subsequent treatment with sodium acetylacetonate in acetone gave the target dinuclear complex

$Pt_2L(acac)_2$ in 43 % overall yield from H_2L.[48] The identity and purity of the complex were characterised by a combination of ^1H NMR spectroscopy in solution, mass spectrometry, elemental analysis and X-ray crystallography (see Experimental section and the Supporting Information).

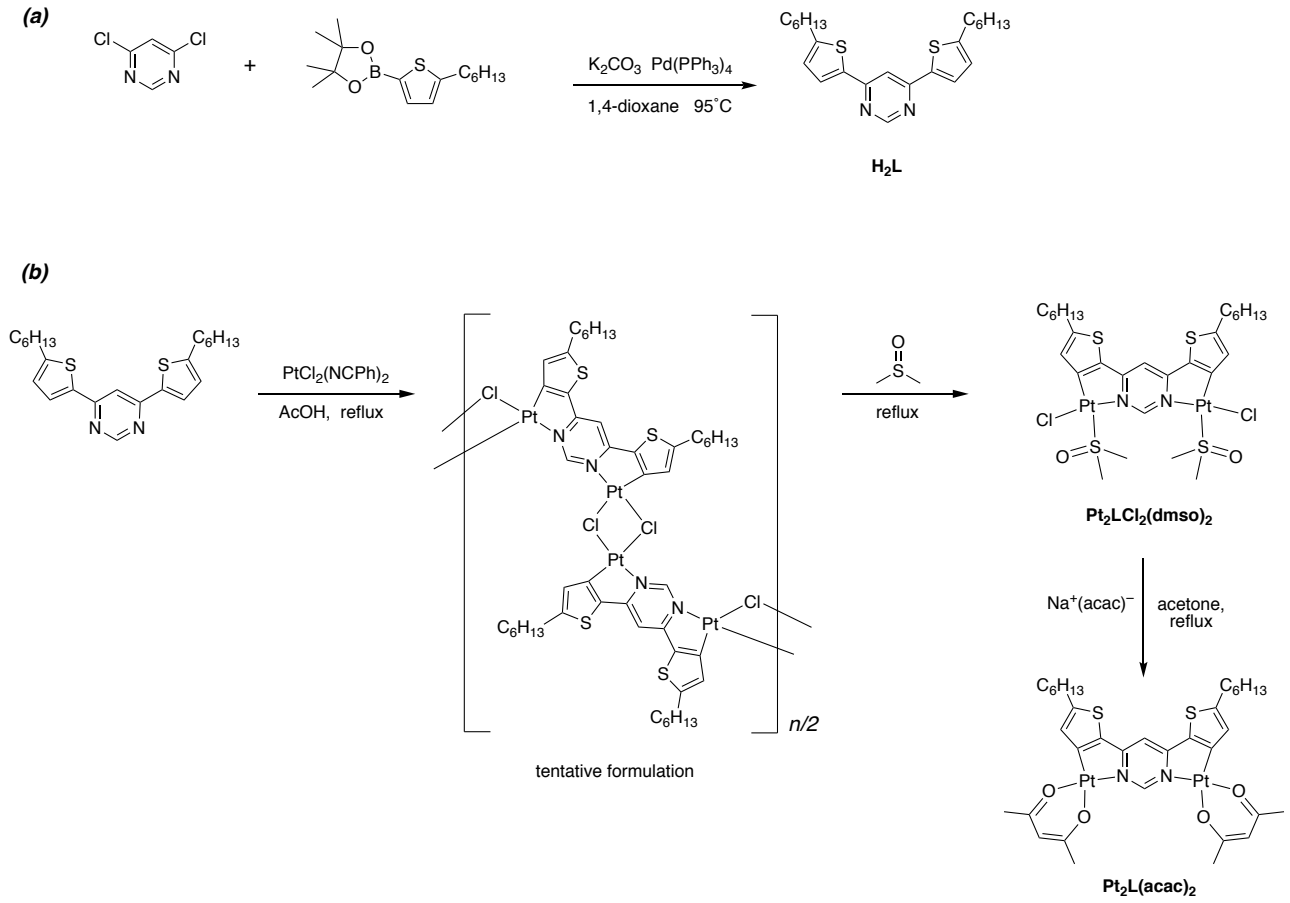

Scheme 1 *(a) Synthesis of the proligand H_2L from 4,6-dichloropyrimidine. (b) Synthesis of the dinuclear complex $Pt_2L(acac)_2$ from H_2L, showing a possible formulation of the initially formed highly insoluble material from which the final product is subsequently obtained.*

(iii) Structure in the solid state

Crystals of $Pt_2L(acac)_2$ suitable for X-ray diffraction analysis were obtained by slow diffusion of methanol into a solution of the complex in dichloromethane. The molecular structure determined is shown in Figure 2. Metal–ligating atom bond lengths for the two Pt(II) centres are listed in Table 1; a comprehensive list of bond lengths and angles and comparison with calculated data are provided in

Table S1 of the Supporting Information. It can be seen that corresponding platinum–ligating atom bond lengths are the same (within about 2 standard deviations) for the two metal centres, and in all cases similar to those in related mononuclear Pt(*N^C*)$_2$(*O^O*) complexes that have been structurally characterised.[35,49] As in such mononuclear cases, the Pt–C bonds are slightly shorter than the Pt–N bonds, whilst the Pt–O bonds that are *trans* to the cyclometallated carbon are elongated relative to those that are *trans* to the pyridines, reflecting the high *trans* influence associated with cyclometallation. The core of the complex is close to being planar, with just a small twist of one of the acac ligands out of the pyrimidine plane: the C4-N2-Pt2-O3 torsion angle is 7.0(3)˚ {as opposed to 0.4(3)˚ for the C3-N1-Pt1-O2}.

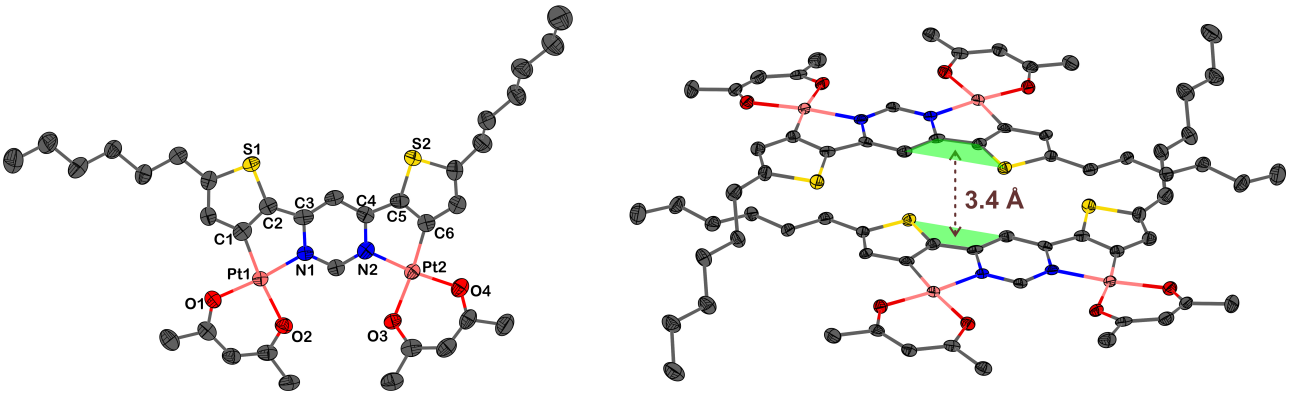

Figure 2 Left: *Molecular structure of Pt$_2$L(acac)$_2$ in the crystal at T = 123 K including the atom numbering scheme for the data in Table 1.* ***Right:*** *Crystal packing structure of the complex. Thermal ellipsoids are shown at 50% probability level and hydrogen atoms are omitted for clarity.*

Table 1 *Metal–ligating atom bond lengths for the two Pt centres in Pt$_2$L(acac)$_2$*

Pt1–ligating atom	***Bond length / Å***	***Pt2–ligating atom***	***Bond length / Å***
C1	*1.957(4)*	*C6*	*1.960(4)*
N1	*1.989(4)*	*N2*	*2.006(4)*
O1	*1.990(4)*	*O4*	*2.003(4)*
O2	*2.061(3)*	*O3*	*2.069(3)*

(iv) Electrochemistry

The electrochemistry of $Pt_2L(acac)_2$ was examined by cyclic voltammetry in dichloromethane solution in the presence of $Bu_4N^+BF_4^-$ as the supporting electrolyte. The complex shows chemically reversible first oxidation and first reduction cycles, $E_{½}^{ox}$ = 0.15 and $E_{½}^{red}$ = –1.84 V, with corresponding onset potentials of 0.06 and –1.77 V respectively (Figure 3). Reversible reduction of cyclometallated complexes featuring aryl-N-heterocycle ligands (*e.g.*, ppy) is commonly encountered, with the reduction process being centred largely on the N-heterocyclic ring with its relatively low-lying LUMO.[50] The reduction potential is somewhat less negative than related mononuclear complexes with either pyridine or pyrimidine rings, for which the corresponding values are typically between about –2.0 and –2.2 V, which may be attributed to a stabilisation of the LUMO through coordination of the second metal centre to the pyrimidine ring. On the other hand, it is unusual for the oxidation of Pt(II) complexes to be reversible, since the resulting d^7 Pt(III) species are susceptible to attack through the axial positions of the square planar system.[51] The observation of a reversible first oxidation implies that the HOMO may be heavily localised on the ligand with little contribution from the metal atom(s).

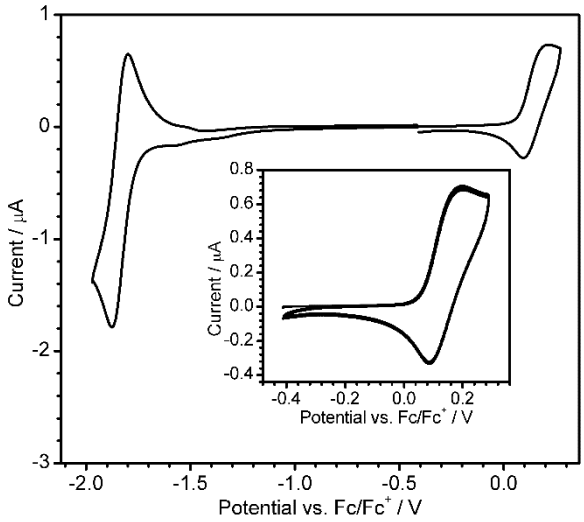

Figure 3 *Cyclic voltammogram of $Pt_2L(acac)_2$ in CH_2Cl_2 (1 mM) in the presence of $Bu_4N^+BF_4^-$ (100 mM) at 295 K. Potentials are relative to the Fc | Fc^+ redox couple half-wave potential. The inset shows three consecutive cycles of the first oxidation process.*

Two further quasi-reversible oxidations are readily resolved at more positive potentials, at $E_{½}^{ox} = 0.43$ and approximately 0.64 V respectively (Figure S1 in the Supporting Information). These processes may be associated with oxidation of the Pt(II) centres, but again, the observation of three as opposed to two oxidations, together with their reversible nature, implies a substantial degree of covalency and extensive delocalisation of the higher occupied orbitals over the metals and ligand.

(v) UV-visible absorption

The UV-visible absorption spectrum of $Pt_2L(acac)_2$ is shown in Figure 4; corresponding numerical data are compiled in Table 2 together with data for Pt(thpy)(acac) for comparison. A striking feature of the spectrum is the remarkably high intensity of the lowest-energy absorption band (λ_{max} = 500 nm), with an extinction coefficient > 5×10^4 M^{-1} cm^{-1}. It exceeds in intensity all other bands in the region investigated (down to 230 nm), a highly unusual observation for cyclometallated metal complexes, where bands in the UV region are normally significantly more intense than those in the visible region. This band is evidently due to charge-transfer transitions that arise as a result of cyclometallation, since the absorption spectrum of the proligand H_2L shows no bands in the visible region: its lowest-energy band is centered at 355 nm (Figure S2 in the Supporting Information). An element of metal-to-ligand charge transfer (MLCT) character might seem likely. However, the planarisation of the organic unit that accompanies the binding of the two metal ions, coupled with an increase in electron density in the phenyl rings upon metallation and the coordination of the heterocycle to two Pt(II) cations, may result in significant intraligand charge transfer (ILCT) character. Such an assignment is supported by the reversibility of the first oxidation process described above, and further discussion follows in Section (vii) in the context of TD DFT results. The lowest-energy band in the dinuclear complex $Pt_2L(acac)_2$ is not only substantially red-shifted but also hugely augmented in intensity compared with that of the mononuclear analogue Pt(thpy)(acac), for which λ_{max} = 421 nm, ε = 4640 M^{-1} cm^{-1}. Close inspection

of the low-energy tail of the spectrum of $Pt_2L(acac)_2$ also reveals a weak band at 590 nm (ε = 360 M^{-1} cm^{-1}), which is attributed to the direct $S_0 \rightarrow T_1$ transition promoted by the spin-orbit coupling associated with the metal centres.[52]

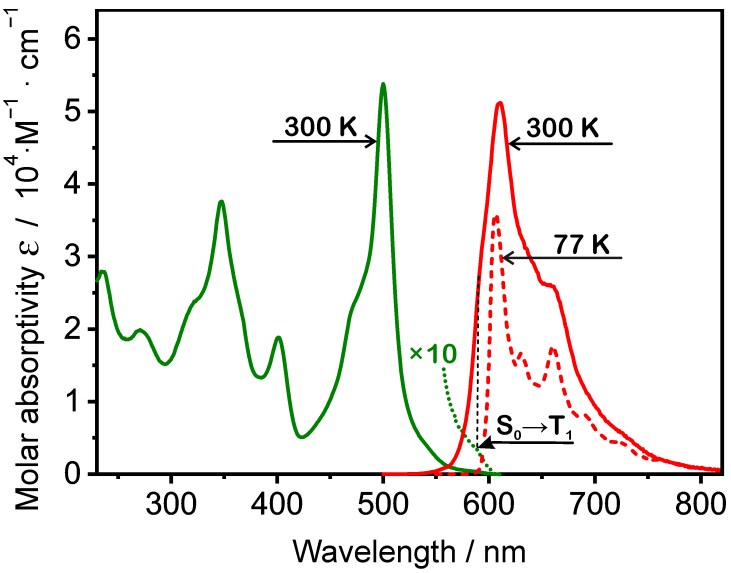

Figure 4 *Absorption spectrum of $Pt_2L(acac)_2$ in CH_2Cl_2 at 300 K (solid green line), including an expansion of the low-energy region highlighting the spin-forbidden $S_0 \rightarrow T_1$ transition (dotted green line); emission spectra of the complex under the same conditions (solid red line) and at 77 K (dashed red line) on an arbitrary intensity axis.*

Table 2. Photophysical properties of $Pt_2L(acac)_2$ in CH_2Cl_2 except where stated otherwise

		$Pt_2L(acac)_2$	**Pt(thpy)(acac)** [(a)]
Absorption 300 K λ_{max} / nm (ε / M^{-1} cm^{-1})		500 (53800), 470 (22400), 400 (18700), 347 (37600), 270 (19900), 235 (27900)	421 (4640), 403 (5210), 359 (7480), 332 (18000, 316 (17300), 286 (17700)
Emission at 300 K	λ_{max} / nm	610, 660sh	554, 556, 602, 654
	τ / μs	12	21
	Φ_{PL} [(b)]	0.85	0.36
	k_r / 10^3 s^{-1}	71	17
	Σ k_{nr} / 10^3 s^{-1}	13	30
Emission at 77 K	λ_{max} / nm	607, 630, 660	549, 571, 596, 622, 652
	τ / μs	26[(c,d)]	23[(e)]
	Φ_{PL}	0.75[(c,d)]	n/a

(a) Data from ref. 11. *(b)* The quantum yield of luminescence were measured using an integrating sphere; see Experimental Section for details. *(c)* In toluene. *(d)* For corresponding data in toluene at 300 K, τ = 10 μs and Φ_{PL} = 0.80. *(e)* In diethyl ether / isopentane / ethanol (2:2:1 v/v).

(vi) Photoluminescence

$Pt_2L(acac)_2$ is intensely luminescent in the red region of the spectrum in deoxygenated solution at ambient temperature, λ_{max} = 610 nm, tailing into the near infrared (NIR) (Figure 4 and Table 2). The spectrum shows evidence of some vibrational structure, and the 0,0 component is displaced by only about 550 cm^{-1} from the triplet absorption band, suggesting little distortion in the T_1 excited state relative to the S_0. Consistent with this conclusion is the observation that the 0,0 component of the spectrum at 77 K is blue-shifted by only a few nm relative to that at 300 K, the only significant difference at the lower temperature being that somewhat more vibrational structure is resolved.

The photoluminescence quantum yield at 300 K is remarkably high for a red emitter, Φ_{PL} = 0.85. Such a high efficiency is rarely encountered for Pt(II) complexes, even when emitting in the green region, and appears to be unprecedented for such a deep red Pt(II)-based emitter.[53] The lifetime of the

luminescence is 12 μs. Assuming that the emitting triplet state is formed with unitary efficiency upon light absorption, the rate constants of radiative, k_r, and non-radiative decay processes, Σk_{nr}, can be estimated through the relationships $k_r = \Phi_{PL} / \tau$ and $k_{nr} = (1/\tau - k_r)$ (Table 2). It may be noted that the value of Σk_{nr} of 1.3×10^4 s^{-1} is less than half that of the corresponding mononuclear complex Pt(thpy)(acac), *even though the emissive excited state of the former lies some 1700 cm^{-1} lower in energy than the latter*. Normally, within a family of structurally related systems, non-radiative decay rates are expected to increase, as the probability of intramolecular energy transfer into vibrations increases in line with the energy gap law.[11,54] Apparently, the dinuclear design of $Pt_2L(acac)_2$ – wherein the pyrimidine core of the ligand is coordinated to two metal centres – rigidifies the molecular structure, thus suppressing the non-radiative relaxation. The importance of rigidity in optimising the luminescence efficiency of Pt(II) complexes has emerged from numerous studies, for example, on the superior performance of complexes with tri- and tetradentate ligands compared to analogues with bidentate ligands.[55,56,57,58,59]

Perhaps even more striking is the observation that the value of k_r of 7.1×10^4 s^{-1} is over 4× higher than that of Pt(thpy)(acac). In our earlier work, we found that an increase in conjugation of the chromophoric ligand from Pt(thpy)(acac) to Pt(dthpy)(acac) (Figure 1), in an effort to red-shift the phosphorescence, was accompanied by a significant slowdown in both intersystem crossing and phosphorescence, reflecting decreased efficiency of SOC as the excited state became more ligand-localised.[22] In contrast, in $Pt_2L(acac)_2$, SOC clearly remains highly efficient, since there is no ligand fluorescence and k_r for phosphorescence is very high. This observation suggests that the presence of a second metal centre allows the T_1 state to couple effectively with higher-lying states of the singlet manifold via SOC, promoting emission. In order to elucidate the pathways by which this may occur,

detailed studies using cryogenic spectroscopy have been carried out along with TD-DFT calculations, as discussed in the sections that follow.

(vii) Cryogenic spectroscopy

The relaxation of the $\Delta S = 0$ spin-selection rule that is necessary to promote the $T_1 \rightarrow S_0$ phosphorescence process is brought about through coupling with higher-lying singlet states by SOC. The three substates of T_1 are non-degenerate and may couple with different efficiencies to the singlet states. Empirically, from studies on a large number of systems, it has been found that the radiative decay rate correlates with the magnitude of the zero-field splitting (ZFS), namely, the difference in energy between the highest- and lowest-lying triplet substates.[5,60,61,62] It was therefore of interest to measure ZFS for $Pt_2L(acac)_2$. In some cases, the substates can be directly resolved from high-resolution emission spectra obtained at liquid helium temperatures in Shpol'skii matrices. In the present case, the spectra recorded at 1.7 and 10 K feature more well-defined vibrational structure than at 77 K, but there is too much broadening for the substates to be resolved (Figure S3 in Supporting Information). However, despite the insufficient spectral resolution, the energy gaps between the substates can instead be estimated from a global fitting of the temperature dependence of the emission decay time over a wide temperature range.[63,60] The variation of τ with T reflects the thermal population of the individual substates – determined by their relative energies – and their individual emission decay times.

In the present study, the temperature dependence of the emission decay time in toluene was investigated over the range $1.7 \leq T \leq 120$ K. Representative emission decay plots are shown in Figure 5a, and the plot of τ against T in Figure 5b. The decay time at $T = 1.7$ K is 280 μs. At this temperature, the emission is essentially exclusively from triplet substate I (Figure 6). The value decreases steeply

with increasing temperature up T = 5 K, as substate II becomes thermally populated, opening up II → S_0 as an additional radiative pathway. The decrease in τ subsequently slows down: at T = 6 K, τ = 253 μs, which probably represents the average decay time of substates I and II. Subsequently, increase in temperature causes τ to drop by an order of magnitude (*e.g.*, at T = 77 K, τ = 26 μs), as a result of thermal population of substate III and opening up of the III → S_0 radiative channel.

The thermally averaged decay time τ(T) at a given temperature T can be expressed by Equation (1), which takes into account the thermal population of the higher-lying substates through a Boltzmann relationship.

$$\tau(T) = \frac{1+ \exp\frac{-\Delta E(\mathrm{II-I})}{k_B T}+\exp\frac{-\Delta E(\mathrm{III-I})}{k_B T}}{\frac{1}{\tau(\mathrm{I})}+\frac{1}{\tau(\mathrm{II})}\exp\frac{-\Delta E(\mathrm{II-I})}{k_B T}+\frac{1}{\tau(\mathrm{III})}\exp\frac{-\Delta E(\mathrm{III-I})}{k_B T}} \qquad (1)$$

Here, τ(I), τ(II), and τ(III) are the decay times of the three substates I, II, and III of the lowest-lying triplet state T_1, respectively; ΔE(II–I) and ΔE(III–I) are the energy gaps between the substates I and II and between I and III, respectively; and k_B is the Boltzmann constant (1.38×10^{-23} J K^{-1}). The experimentally determined data points of Figure 5b were fitted to Equation (1) by fixing τ(I) as 280 μs (namely the value at 1.7 K). The best fit is shown by the red line in Figure 5b, leading to τ(II) = 200 μs and τ(III) = 6 μs, and values of ΔE(II–I) = 4 cm^{-1} and ΔE(III–I) = ΔE(ZFS) = 40 cm^{-1} (as illustrated in Figure 6). The ZFS value of 40 cm^{-1} is remarkably high for a complex of a d^8 metal ion. For comparison, Pt(thpy)(acac) has ZFS = 4.3 cm^{-1} and the bright-green emitting Pt(dfdpyb)Cl (one of the brightest known mononuclear Pt(II) complexes) has a ZFS value of 11.3 cm^{-1} (dfdpybH = 4,6-difluoro-1,3-dipyridylbenzene).[60,63] Only for complexes of third-row d^6 metals {Ir(III) and Os(II)} have ZFS values in excess of 50 cm^{-1} been found.[5,36] The large ZFS is consistent with efficient SOC of the T_1

state with states of the singlet manifold, which leads to the observed high rate constant k_r of the $T_1 \rightarrow S_0$ phosphorescence process.

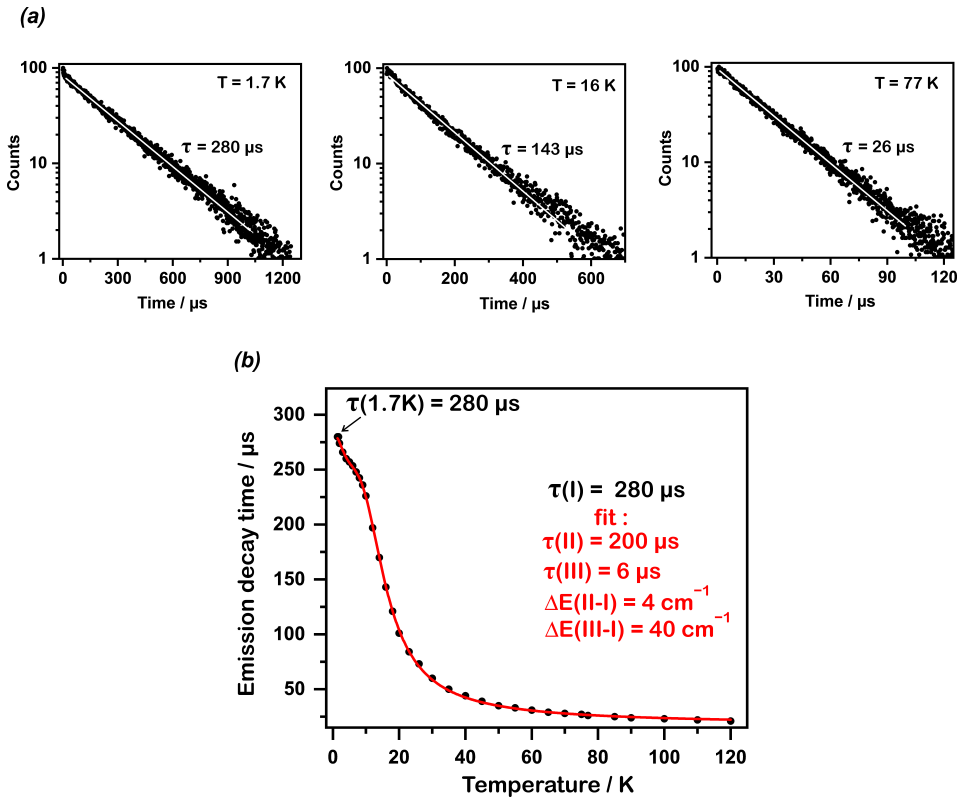

Figure 5 *(a) Representative emission decay traces (logarithmic y axis) of $Pt_2L(acac)_2$ in toluene (10^{-5} M) measured at T = 1.7 K, 16 K, and 77 K. (b) Plot of the experimentally measured emission decay times as a function of temperature (black dots) together with the best fit of the data points to Equation (1) (red line).*

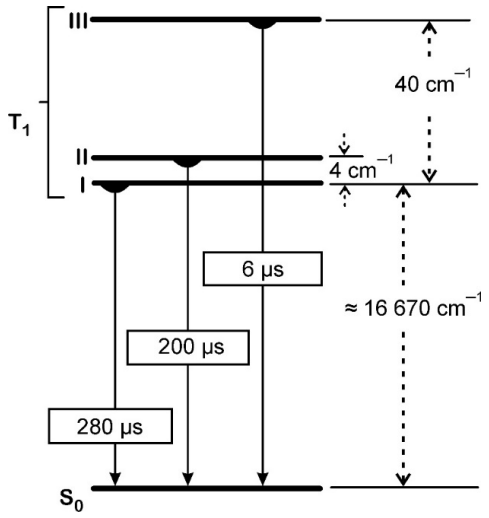

Figure 6. *Schematic energy level diagram of the emitting triplet state and individual emission decay times of the T_1 substates I, II, and III of $Pt_2L(acac)_2$ in toluene (not to scale).*

(viii) Density functional theory calculations

Calculations were carried out on a model structure closely related to $Pt_2L(acac)_2$ but in which the hexyl chains were truncated to methyl groups – denoted $Pt_2L^{Me}(acac)_2$. The electronic structure was analysed using Gaussian 09 [64] at the M06/def2-SVP level, with a CPCM model for dichloromethane as the solvent. The optimized geometry determined for the S_0 ground state is consistent with the X-ray diffraction data (Table S1 in the Supporting Information), whilst TD-DFT calculations at the S_0 geometry give transition energies and oscillator strengths that agree well with the profile of the experimental absorption spectrum (Table S2 in the Supporting Information). The S_1 state has almost exclusively HOMO → LUMO character (Table S4 in Supporting Information), and the corresponding orbitals (Table S6) are delocalised over both of the thienyl rings and the central pyrimidine, accounting for the low energy of the lowest-energy absorption bands in $Pt_2L(acac)_2$. Moreover, the oscillator strength of the $S_0 \rightarrow S_1$ transition in $Pt_2L^{Me}(acac)_2$ is seen to be remarkably large, $f = 0.6023$ at the S_0 geometry (Table S2), which is consistent with the unusually high intensity of the experimentally observed band at λ_{max} = 500 nm in $Pt_2L(acac)_2$ (Figure 4). The calculations show a strong spatial

overlap of the orbitals involved in the $S_0 \rightarrow S_1$ transition (*i.e.*, of the HOMO and LUMO) yet which have major contributions from different atoms, two key requirements for a strong transition dipole moment and high intensity of absorption.

In seeking insight into emission properties, the lowest triplet state T_1 must be considered (the geometry parameters for which are given in Table S1; note that unlike S_1, the T_1 geometry is slightly asymmetric). TD-DFT calculations at the T_1 geometry show that the state has predominantly HOMO → LUMO character (82%) with minor contributions from HOMO–1 → LUMO (6%), HOMO → LUMO+1 (3%) and HOMO–3 → LUMO (2%) (Table S3 in the Supporting Information). Inspection of the pertinent orbitals confirms that the excited states can be viewed as being primarily ligand-centred, with admixtures of MLCT character (Figure 7; population analysis in Supporting Information). It may be noted that the orbitals HOMO, HOMO–1 and HOMO–3 involve Pt d orbitals of different m_ℓ value; in other words, T_1 differs from S_1 in terms of the participating d orbitals. As noted above, the S_1 state – the closest-lying singlet with which T_1 could mix through SOC – is almost exclusively HOMO → LUMO. A key requirement for effective SOC in metal complexes is that the triplet state can mix with a ^{1}MLCT state that involves *different* d orbitals – a requirement that is evidently fulfilled here.[5,36,63] In $Pt_2L(acac)_2$, *both* of the Pt(II) ions contribute to HOMO, as well as HOMO–1 and HOMO–3, which may further facilitate SOC between T_1 and S_1. Moreover, as noted above, the oscillator strength of the $S_1 \rightarrow S_0$ transition is particularly high, even at the T_1 geometry (f = 0.5736, Table S3), and so a high $T_1 \rightarrow S_0$ phosphorescence rate could be anticipated, as is indeed observed experimentally.

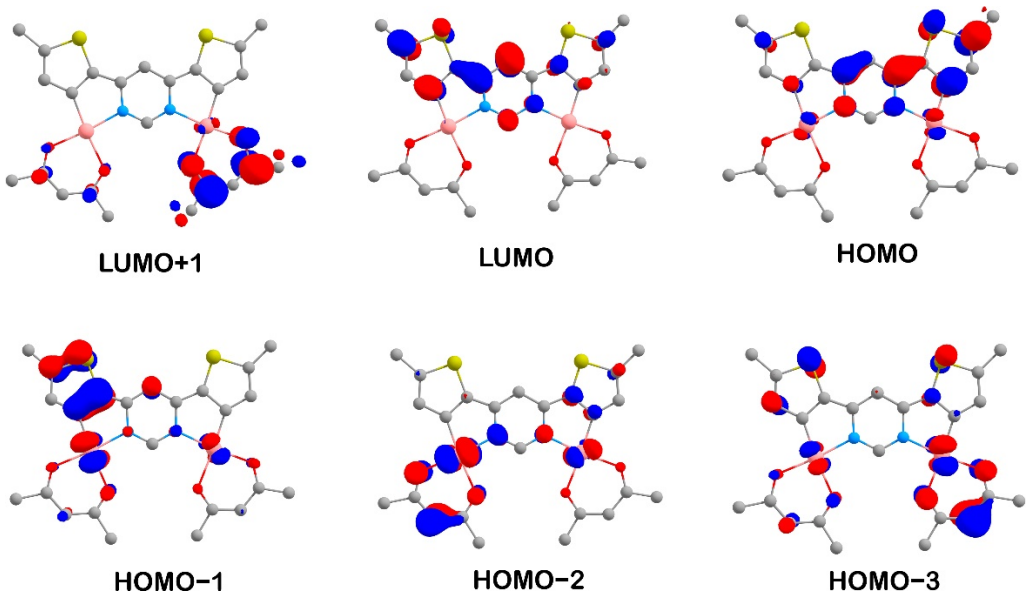

Figure 7 *Contour plots of molecular orbitals contributing to the T_1 state of $Pt_2L^{Me}(acac)_2$ calculated at the T_1 geometry (iso value = 0.05).*

(ix) OLED devices

Using $Pt_2L(acac)_2$ as a phosphorescent dopant, we fabricated solution-processed multilayer OLED devices (Figures 8 and 9). The complex has sufficient solubility for spin-coating from a toluene solution containing the host materials *N*,*N*'-bis(3-methylphenyl)-*N*,*N*'-diphenylbenzidine (TPD) and 2-(4-biphenyl)-5-(4-*tert*-butylphenyl)-1,2,4-oxadiazole (PBD). They function to improve charge injection, acting as hole- and electron-transport materials respectively, with IP = 5.3 eV and EA = 2.7 eV respectively. These values match well the respective parameters of the dopant (IP = 5.16 eV, EA = 3.33 eV). High molecular weight poly(*N*-vinylcarbazole) (PVK) was used as an electron-blocking layer in order to improve device efficiency by reducing current leakage.[65,66] The overall structure of the device was: ITO | HIL 1.3N (45 nm) | PVKH (10 nm) | TPD:PBD (60:40) co 5% $Pt_2L(acac)_2$ (30 nm) | TPBi (50 nm) | LiF (0.8 nm) | Al (100 nm) (Figure 8). The device shows red electroluminescence with a high maximum brightness (4450 cd m^{-2}) and radiosity (7.2 mW cm^{-2}), attaining 9.9 % EQE with λ_{EL} = 612 nm (CIE coordinates: x = 0.64, y = 0.34) (Figure 9). The Φ_{PL}= 0.30 ± 0.04 (λ_{exc} = 500 nm) of the $Pt_2L(acac)_2$-doped TPD:PBD blend, measured in a nitrogen atmosphere, is consistent with the

maximum EQE achieved in the OLED, assuming a light out-coupling limit of 30 to 40%. The lower PLQY of emission from the film compared to degassed solution is most likely due to intermolecular interactions, either in the ground or excited state or both, as often found for other triplet emitters in films albeit normally at higher doping concentrations. Such interactions may be facilitated here by the extended planar nature of the molecules.

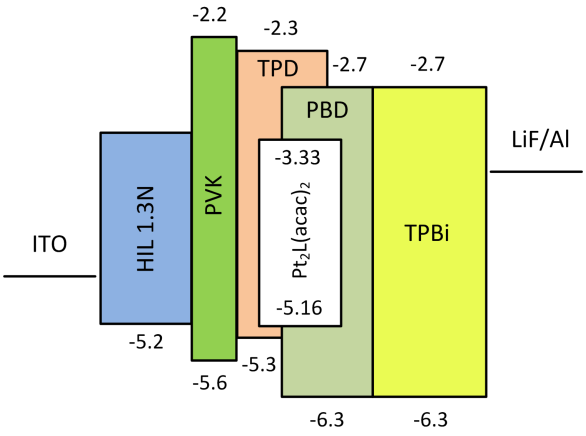

Figure 8 *Structure of the OLED device. TPBi = 1,3,5-(benzinetriyl)-tris(1-phenyl-1-H-benzimidazole); HIL 1.3N is a propietary form of poly(3,4-ethylenedixoythiophene) polystyrene sulfonate (PEDOT); ITO = indium tin oxide; other abbreviations are given in the text.*

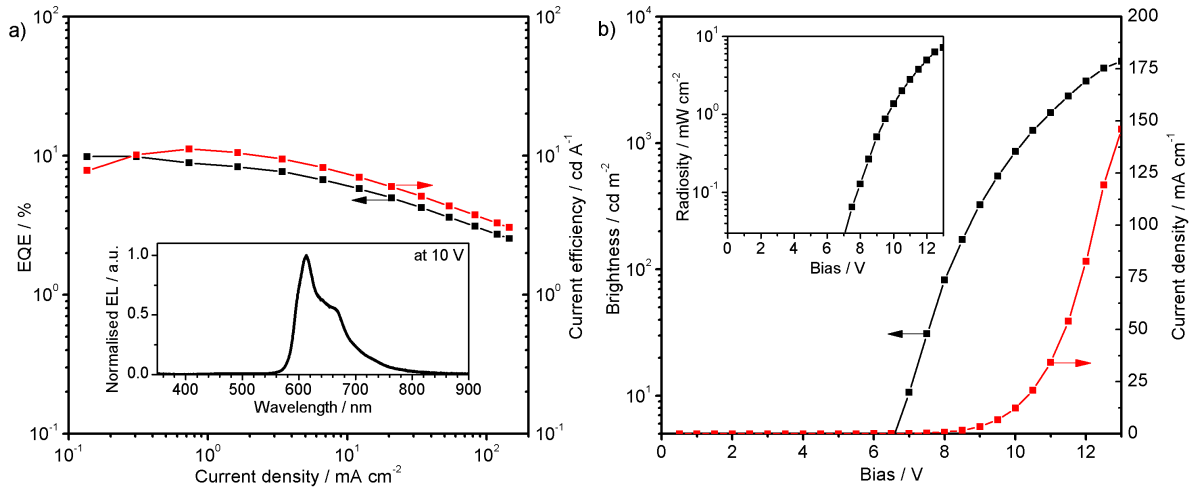

Figure 9 *Device characteristics of the solution-processed OLED prepared using $Pt_2L(acac)_2$ as the phosphorescent dopant: (a) EQE and current efficiency vs current density (inset: electroluminescence spectrum); (b) brightness and current density vs bias (inset: radiosity vs bias).*

To put the device results in context, it is important to note that the vast majority of efficient phosphorescent OLEDs employ iridium-based emitters, rather than those based on platinum; *e.g.*, the red-emitting $Ir(mphq)_2(acac)$ and $Ir(piq)_2(acac)$ {mphq = 2-(3,5-dimethylphenyl)quinoline, piq = 1-phenyl-isoquinoline}[67,68,69] and Ir(III) complexes with more esoteric ligands such as spirofluorene-quinoxalines.[70] Inevitably, it is in devices prepared by vacuum sublimation that the highest efficiencies are achieved, but an impressive EQE of 19.3% has been reported recently for a solution processed red-emitting OLED based on an iridium complex.[71] Some impressive results have also been obtained reccently using purely organic emitters.[72] Amongst Pt(II)-based devices, on the other hand, vacuum-deposited OLEDs have recently reached an EQE of around 20% in the red / NIR,[73] but, for a solution-processed deep-red-emitting Pt(II)-based device, the EQE of almost 10% obtained here renders it amongst the highest reported.[74,75,76]

CONCLUSION

In summary, this study shows how the use of bis-cyclometallating ligands to generate dinuclear complexes offers an appealing strategy to obtain molecular materials that emit with high efficiency in the red region of the spectrum. The high efficiencies arise from the combination of suppressed non-radaitive decay pathways and an enhanced radiative rate constant. The former may be associated with the highly rigid nature of the structure arising from the binding of two metal ions. The origin of the latter has been probed through temperature-dependent studies down to 1.7 K, which have revealed an unusually large zero-field splitting of the triplet state for a Pt(II)-based complex, suggesting very efficient spin-orbit coupling pathways. TD-DFT results indicate that the triplet state can mix with a ^{1}MLCT state that involves different d orbitals, satsifying a key requirement for effective SOC.

The results point towards an effective approach for essentially circumventing the troublesome trend to lower phosphorescence efficiencies as excited-state energy decreases, and hence to superior red and NIR-emitting phosphors, for example as demonstrated here for OLEDs. The augmentation in emission efficiency is accompanied by unusually intense low-energy absorption, with ε values in the visible region at 500 nm higher even than those in the far-UV. Thus, the resulting "brightness" (defined as $\varepsilon \times \Phi_{PL}$) is exceptionally high for a visibly-excited phosphorescent molecule. Such attributes are of particular importance in the application of light-emitting molecules to other areas of science. For example, in bio-imaging, long-wavelength excitation coupled with emission in the red or NIR – in which regions biological tissue is most transparent to light – is especially desirable.[9,10]

EXPERIMENTAL SECTION

(i) General

Commercially available reagents were used as received from suppliers without further purification unless otherwise specified. Reactions were monitored by TLC using silica gel with UV254 fluorescent indicator. NMR spectra were recorded on a JEOL ECS400FT Delta spectrometer (399.78 MHz for ^{1}H NMR, 100.53 MHz for ^{13}C NMR). Chemical shifts are reported in parts per million (ppm). Coupling constants (J) are measured in Hertz. High resolution mass spectra were obtained on a Thermo Scientific™ LTQ Orbitrap XL™ spectrometer using nano-electrospray ionisation at the EPSRC National Mass Spectrometry Service, Swansea.

(ii) Optical spectroscopy

UV-Vis absorption spectra were measured using a Varian Cary 300 double beam spectrometer with the sample held in a quartz cuvette of pathlength 1 cm. Spectra were recorded against pure solvent in an optically matched cuvette. Emission spectra were measured with a Jobin Yvon Fluorolog 3 steady-state fluorescence spectrometer. For variable-temperature measurements, the sample was deposited in a helium cryostat (CryoVac KONTI IT) in which the helium gas flow, gas pressure, and heating were controlled to allow the temperature to be regulated between 1.6 and 300 K. Photoluminescence quantum yields were determined with a Hamamatsu C9920-02 system equipped with a Spectralon® integrating sphere. For decay time measurements, a PicoBright PB-375L pulsed diode laser (λ = 378

nm, pulse width 100 ps) was applied as the excitation source. The emission signal was detected with a cooled photomultiplier attached to a FAST ComTec multichannel scalar card with a time resolution of 250 ps.

(iii) Electrochemistry

Cyclic voltammetry was conducted in three-electrode, one-compartment cell. All measurements were performed at room temperature in dichloromethane (ExtraDry AcroSeal®, Acros Organics) in the presence of Bu_4NBF_4 (0.1 M, 99%, Sigma Aldrich, dried). Solutions were nitrogen-purged prior to measurements. A Pt disc working electrode (1 mm^2) and Pt wire counter electrode were used, with a Ag|AgCl reference electrode (calibrated against ferrocene); measurements were recorded at a scan rate of 50 mV s^{-1}. The ionization potential (IP) and electron affinity (EA) were determined from the respective onset potentials using a well-established relationship: IP = E_{onset}^{ox} + 5.1; EA = E_{onset}^{red} + 5.1.[77]

(iv) Computations

All calculations were carried out with the Gaussian 09 package utilizing DFT approach with M06 functional and def2-SVP basis set including ECPs for Pt(II) ion. Geometry optimizations were conducted with "very tight" criteria. The CPCM solvation model was applied with solvent parameters for dichloromethane.

(v) Device fabrication and evaluation

OLEDs were fabricated by spin-coating / evaporation hybrid method. The hole injection layer (Heraeus Clevios HIL 1.3N), electron blocking/hole transport layer (PVKH), and emitting layer (TPD:PBD + dopant) were spin-coated, whereas the electron transport layer (TPBi) and cathode (LiF/Al) were evaporated. Devices of 4 × 2 mm pixel size were fabricated. TPD - *N*,*N*'-bis(3-methylphenyl)-*N*,*N*'-diphenylbenzidine (sublimed, LUMTEC), PVKH – poly(9-vinylcarbazole) (MW = 1 100 000, Sigma Aldrich), PBD - 2-(biphenyl-4-yl)-5-(4-*tert*-butylphenyl)-1,3,4-oxadiazole (99%, Sigma Aldrich), TPBi - 2,2',2''-(1,3,5-Benzinetriyl)-tris(1-phenyl-1-*H*-benzimidazole) (sublimed, LUMTEC), LiF (99.995%, Sigma Aldrich), and aluminium wire (99.9995%, Alfa Aesar) were purchased from the suppliers indicated in parentheses. OLED devices were fabricated using pre-cleaned indium tin oxide (ITO)-coated glass substrates after ozone plasma treatment, with a sheet resistance of 20 Ω cm^{-2} and ITO thickness of 100 nm. Heraeus Clevios HIL 1.3N was spun-coated and annealed onto a hotplate at 200°C for 3 min to give a 45 nm film. The electron blocking / hole

transport layer (PVKH, 3 mg/mL), was spun from a chloroform:chlorobenzene (95:5 v/v) mixture and annealed at 50°C for 5 min to give a 10 nm film. The emitting layer was spun from a toluene solution of TPD:PBD (60:40 w/w) with total concentration of 10 mg/mL. The dopant was dissolved in the host solution to give a final concentration of 5% in the emitting layer. This solution was spun onto the PVKH layer and then annealed at 50°C for 5 min giving a 30 nm film. All solutions were filtered directly before application using a PVDF syringe filter with 0.45 μm pore size. All other organic and cathode layers were thermally evaporated using Kurt J. Lesker Spectros II deposition system at 10^{-6} mbar. Organic materials and aluminum were deposited at a rate of 1 Å s^{-1}, whereas the LiF layer was deposited at 0.1–0.2 Å s^{-1}. Characterisation of OLED devices was conducted in a 10-inch integrating sphere (Labsphere) connected to a Source Measure Unit.

(vi) Crystallography

A clear orange plate-shaped crystal with dimensions $0.22 \times 0.16 \times 0.08$ mm^3 was mounted on a MITIGEN holder with inert oil. X-ray diffraction data were collected using a SuperNova, Single source at offset, Eos diffractometer equipped with a low-temperature device, operating at T = 123.08(13) K. Data were measured using scans of 0.5° per frame for 25 s using MoK_α radiation (micro-focus sealed X-ray tube). The total number of runs and images was based on the strategy calculation from the program CrysAlisPro (Agilent). The maximum resolution achieved was 29.224°. Cell parameters were retrieved and refined using CrysAlisPro (Agilent) on 15632 reflections, 29 % of the observed reflections, and data reduction was performed using the same software, correcting for Lorentz polarisation. The structure was solved in the space group $P2_1/c$ (# 14) by intrinsic phasing using the **ShelXT** (Sheldrick, 2015) structure solution program and refined by least squares using version 2014/7 of **ShelXL** (Sheldrick, 2015). All non-hydrogen atoms were refined anisotropically. Hydrogen atom positions were calculated geometrically and refined using the riding model. Formula = $C_{34}H_{44}N_2O_4Pt_2S_2$; formula weight = 999.01; colour = clear orange; crystal system = monoclinic; space group = $P2_1/c$; Z = 4; unit cell parameters: a = 21.3046(3) Å, b = 7.7920(1) Å, c = 20.9345(2) Å, α = 90°, β = 94.210(1)°, γ = 90°; final R indices: R1 = 0.0335, wR2 = 0.0709. Goodness-of-fit = 1.088. The crystallographic data are available in cif format as Supporting Information and have been deposited at CCDC, under the code 1863253.

(vii) Synthetic procedures and characterisation data

4,6-Bis(5-hexylthiophen-2-yl)pyrimidine H_2L

A mixture of 4,6-dichloropyrimidine (0.392 g, 2.61 mmol), 5-hexyl-2-thiopheneboronic acid pinacol ester (1.96 g, 6.80 mmol), $Pd(PPh_3)_4$ (0.183 g, 0.157 mmol), an aqueous solution of K_2CO_3 (2 M, 7.80 mL, 15.6 mmol) and 1,4-dioxane (20 mL) was deoxygenated by bubbling argon through the mixture for 10 min. The mixture was then stirred at 95°C under argon for 24 h. Upon cooling to room temperature, toluene (15 mL) was added and the solution was washed with water (3 × 10 mL). The organic phase was dried over anhydrous $MgSO_4$, the solvent was removed under reduced pressure, and the residue was recrystallised from ethyl acetate to give the product (0.908 g, 84%). ^{1}H NMR ($CDCl_3$, 400 MHz): δ_H 8.98 (d, 1H, J = 1.2), 7.68 (d, 1H, J = 1.2), 7.65 (d, 2H, J = 3.8), 6.86 (d, 2H, J = 3.8), 2.87 (t, 4H, J = 7.4), 1.76-1.69 (m, 4H), 1.41-1.30 (m, 12H), 0.89 (t, 6H, J = 7.2); ^{13}C NMR ($CDCl_3$, 100 MHz): δ 159.1 (CH), 158.97 (C), 151.71 (C), 139.3 (C), 127.4 (CH), 125.8 (CH), 107.9 (CH), 31.5 (CH_2), 31.4 (CH_2), 30.5 (CH_2), 28.7 (CH_2), 22.6 (CH_2), 14.1 (CH_3).

$Pt_2L(acac)_2$

A mixture of the proligand H_2L (0.134 g, 0.325 mmol) and $PtCl_2(NCPh)_2$ (0.338 g, 0.714 mmol) in acetic acid (80 mL) was heated to reflux under argon for 17 h. Upon cooling to room temperature, the solvent was removed under reduced pressure, and the dark red residue – of probable composition $[Pt_2L(\mu\text{-}Cl)_2]_n$ (Scheme 1) – was filtered and washed successively with methanol (10 mL), water (15 mL) and more methanol (10 mL). The solid was transferred into a round-bottomed flask; DMSO (5 mL) was added and the mixture was heated at reflux under argon for 5 min. The resulting solution was allowed to cool to about 50-60°C, at which point methanol (40 mL) was slowly added. The precipitate that formed was separated by filtration and washed with methanol to give $Pt_2LCl_2(dmso)_2$ (Scheme 1) as a dark red solid. This dmso complex (0.198 g, 0.192 mmol) was placed in a round-bottomed flask, to which was added acetone (100 mL) and sodium acetylacetonate (0.235 g, 1.92 mmol). The mixture was heated at reflux under argon for 6 h. Upon cooling to room temperature, water (100 mL) was added and the dark red solid that formed was filtered off, washed with water and acetone, and purified by column chromatography on silica using DCM as the eluent to give the target complex $Pt_2L(acac)_2$ as a red solid (82 mg, 43%). (^{1}H NMR ($CDCl_3$, 400 MHz): δ_H 9.37 (d, 1H, J = 1.8), 6.87 (s, 2H), 6.70 (d, 1H, J = 1.8), 5.45 (s, 2H), 2.91 (t, 4H, J = 7.6), 1.75-1.67 (m, 4H), 1.42-1.29 (m, 12H), 0.88 (t, 6H, J = 6.8); HRMS (FTMS$^+$): for $[M]^+$ calculated 998.2027, found 998.2031. Elemental analysis: calculated

C 40.88, H 4.44, N 2.80%; found C 40.93, H 4.37, N 2.77 %. HRMS (NESI): for $[M]^+$ calc'd 998.2027, found 998.2031.

ASSOCIATED CONTENT

Supporting Information

Absorption and emission spectra of proligand H_2L; emission spectra of $Pt_2L(acac)_2$ in toluene at 1.7, 10, 77 and 300 K; further information and output parameters of DFT and TD-DFT calculations; ^1H and ^{13}C NMR spectra and mass spectrometric data for $Pt_2L(acac)_2$ and intermediates.

Accession codes

CCDC 1863253 contains the supplementary crystallographic data for this paper. The data can be obtained free of charge via www.ccdc.cam.ac.uk/data_request/cif or by e-mailing data_request@ccdc.cam.ac.uk or by contacting The Cambridge Crystallographic Data Centre, 12 Union Road, Cambridge CB2 1EZ, UK; fax: +44 1223 336033.

AUTHOR INFORMATION

Corresponding Authors

*E-mail: shafikoff@gmail.com

*E-mail: j.a.g.williams@durham.ac.uk

*E-mail: valery.kozhevnikov@northumbria.ac.uk

ORCID

Marsel Z. Shafikov: 0000-0003-0495-0364

J. A. Gareth Williams: 0000-0002-4688-3000

Valery N. Kozhevnikov: 0000-0001-7032-8866

Piotr Pander: 0000-0003-4103-4154

Fernando B. Dias: 0000-0001-9841-863X

Notes

The authors declare no competing financial interest.

ACKNOWLEDGEMENTS

M.Z.S. thanks the German Research Foundation (DFG) for financial support (Project № 389797483), and Professor Duncan Bruce and the University of York, U.K. for use of computational facilities. P.P. acknowledges support from EU Horizon 2020 under the EXCILIGHT project, № 674990. We thank the EPSRC National Mass Spectrometry Service Centre for recording mass spectra and Dr Michael Bodensteiner (University of Regensburg, Central Analytical Services) for the X-ray structure determination. We are grateful to Dr Rafał Czerwieniec and Prof. Dr Hartmut Yersin for many inspiring and informative discussions on the subject of spin-orbit coupling and zero-field splitting.

REFERENCES

1. Highly Efficient OLEDs with Phosphorescent Materials, ed. Yersin, H., Wiley-VCH, Weinheim, Germany, 2007.
2. Chi, Y.; Chou, P. T. Transition Metal Phosphors with Cyclometalating Ligands: Fundamentals and Applications. *Chem. Soc. Rev.* **2010**, *39*, 638-655.
3. Gildea, L.F.; Williams, J.A.G. "Iridium and Platinum Complexes for OLEDs", in *Organic Light-Emitting Diodes: Materials, Devices and Applications,* ed. Buckley, A., Woodhead, Cambridge, 2013, Chapter 3, pp 77-113.
4. Baranoff, E.; Curchod, B.F.E. FIrpic: Archetypal Blue Phosphorescent Emitter for Electroluminescence. *Dalton Trans.* **2015**, *44*, 8318-8329.
5. Yersin, H.; Rausch, A.F.; Czerwieniec, R.; Hofbeck, T.; Fischer, T. The Triplet State of Organo-Transition Metal Compounds. Triplet Harvesting and Singlet Harvesting for Efficient OLEDs. *Coord. Chem. Rev.* **2011**, *255*, 2622-2652.
6. Adachi, C.; Third Generation Organic Electroluminescence Materials. *Jpn. J. Appl. Phys.* **2014**, *53*, 060101.
7. Im, Y.; Kim, M.; Cho, Y.J.; Seo, J.A.; Yook, K.S.; Lee, J.Y. Molecular Design Strategy of Organic Thermally Activated Delayed Fluorescence Emitters. *Chem. Mater.* **2017**, *19*, 1946-1963.
8. Yang, Z.Y.; Mao, Z.; Xie, Z.L.; Zhang, Y.; Liu, S.W.; Zhao, J.; Xu, J.R.; Chi, Z.G.; Aldred, M.P. Recent Advances in Organic Thermally Activated Delayed Fluorescence Materials. *Chem. Soc. Rev.* **2017**, *46*, 915-106.
9. Baggaley, E.; Weinstein, J. A.; Williams, J.A.G. Lighting the Way to See Inside the Live Cell with Luminescent Transition Metal Complexes. *Coord. Chem. Rev.* **2012**, *256*, 1762-1785.
10. Baggaley, E.; Weinstein, J. A.; Williams, J.A.G. Time-Resolved Emission Imaging Microscopy using Phosphorescent Metal Complexes: Taking FLIM and PLIM to New Lengths. *Struct. Bond.* **2015**, *165*, 205-256.
11. Zhao, Q.; Li, F.; Huang, C. Phosphorescent Chemosensors Based on Heavy-Metal Complexes. *Chem. Soc. Rev.* **2010**, *39*, 3007-3030.
12. You, Y.; Cho, S.; Nam, W. Cyclometalated Iridium(III) Complexes for Phosphorescence Sensing of Biological Metal Ions. *Inorg. Chem.* **2014**, *53*, 1804-1815.

13. Williams, J.A.G. “Multinuclear Iridium Complexes”, in Iridium(III) in Optoelectronics and Photonics Applications. Ed. Zysman-Colman, E., John Wiley & Sons Ltd, 2017.
14. Puttock, E.V.; Walden, M.T.; Williams, J.A.G. The Luminescence Properties of Multinuclear Platinum Complexes. *Coord. Chem. Rev.* **2018**, *367*, 127-162.
15. Kozhevnikov, V.N.; Durrant, M.C.; Williams, J.A.G. Highly Luminescent Mixed-Metal Pt(II)/Ir(III) Complexes: Bis-Cyclometalation of 4,6-Diphenylpyrimidine as a Versatile Route to Rigid Multimetallic Assemblies. *Inorg. Chem.* **2011**, *50*, 6304-6313.
16. Lanoë, P.H.; Tong, C.M.; Harrington, R.W.; Probert, M.R.; Clegg, W.; Williams, J.A.G.; Kozhevnikov, V.N. Ditopic Bis-Terdentate Cyclometallating Ligands and their Highly Luminescent Dinuclear Iridium(III) Complexes. *Chem. Commun.* **2014**, *50*, 6831-6834.
17. Daniels, R.E.; Culham, S.; Hunter, M.; Durrant, M.C.; Probert, M.R.; Clegg, W.; Williams, J.A.G.; Kozhevnikov, V.N. When Two Are Better Than One: Bright Phosphorescence from Non-stereogenic Dinuclear Iridium(III) Complexes. *Dalton Trans.* **2016**, *45*, 6949-6962.
18. Turnbull, G.; Williams, J.A.G.; Kozhevnikov, V.N. Rigidly Linking Cyclometallated Ir(III) and Pt(II) Centres: an Efficient Approach to Strongly Absorbing and Highly Phosphorescent Red Emitters. *Chem. Commun.* **2017**, *53*, 2729-2732.
19. Culham, S.; Lanoë, P. H.; Whittle, V.L.; Durrant, M.C.; Williams, J.A.G.; Kozhevnikov, V.N. Highly Luminescent Dinuclear Platinum(II) Complexes Incorporating Bis-Cyclometallating Pyrazine-Based Ligands: A Versatile Approach to Efficient Red Phosphors. *Inorg. Chem.* **2013**, *52*, 10992-11003.
20. Englman, R.; Jortner, J. The Energy Gap Law for Radiationless Transitions in Large Molecules. *Mol. Phys.* **1970**, *18*, 145-164.
21. Brulatti, P.; Gildea R.J.; Howard, J.A.K.; Fattori, V.; Cocchi, M.; Williams, J.A.G. Luminescent Iridium(III) Complexes with N^C^N-Coordinated Terdentate Ligands: Dual Tuning of the Emission Energy and Application to Organic Light-Emitting Devices. *Inorg. Chem.* **2012**, *51*, 3813-3826.
22. Kozhevnikov, D.N.; Kozhevnikov, V.N.; Shafikov, M.Z.; Prokhorov, A.M.; Bruce, D.W.; Williams, J.A.G. Phosphorescence vs Fluorescence in Cyclometalated Platinum(II) and Iridium(III) Complexes of (Oligo)thienylpyridines. *Inorg. Chem.* **2011**, *50*, 3804-3815.
23. Chou, P.T.; Chi, Y.; Chung, M.W.; Lin, C.C. Harvesting Luminescence via Harnessing the Photophysical Properties of Transition Metal Complexes. *Coord. Chem. Rev.* **2011**, *255*, 2653-2665.
24. For a recent review of OLEDs using multinuclear Ir(III) complexes, see: Li, G.; Congrave, D.G.; Zhu, D.; Su, Z.; Bryce, M.R. Recent Advances in Luminescent Iridium(III) Complexes and Their Application in Organic Electroluminescent Devices. *Polyhedron*, **2018**, *140*, 146-157.
25. Ma, B.W.; Djurovich, P.I.; Garon, S.; Alleyne, B.; Thompson, M.E. Platinum Binuclear Complexes as Phosphorescent Dopants for Monochromatic and White Organic Light-Emitting Diodes. *Adv. Funct. Mater.* **2006**, *16*, 2438-2446.
26. Yang, S.; Meng, F.; Wu, X.; Yin, Z.; Liu, X.; You, C.; Wang, Y.; Su, S.; Zhu, W. Dinuclear Platinum(II) Complex Dominated by a Zig-Zag-Type Cyclometalated Ligand: A New Approach to Realize High-Efficiency Near Infrared Emission. *J. Mater. Chem. C*, **2018**, *6*, 5769-5777.

27. Zhang, Y.M.; Meng, F.; Tang, J.H.; Wang, Y.; You, C.; Tan, H.; Liu, Y.; Zhong, Y.W.; Su, S.; Zhu, W. Achieving Near-Infrared Emission in Platinum(II) Complexes by Using an Extended Donor–Acceptor-Type Ligand. *Dalton Trans.* **2016**, *45*, 5071-5080.
28. Flamigni, L.; Barbieri, A.; Sabatini, C.; Ventura, B.; Barigelletti, F. Photochemistry and Photophysics of Coordination Compounds; Iridium. *Top. Curr. Chem.* **2007**, *281*, 143-203.
29. Williams J.A.G. Photochemistry and Photophysics of Coordination Compounds; Platinum. *Top. Curr. Chem.* **2007**, *281*, 205-268.
30. Chou, P.T.; Chi, Y. Phosphorescent Dyes for Organic Light-Emitting Diodes. *Chem. Eur. J.* **2007**, *13*, 380-395.
31. Zhou, G.; Wong, W.Y.; Yang, X. New Design Tactics in OLEDs Using Functionalized 2-Phenylpyridine-Type Cyclometalates of Iridium(III) and Platinum(II). *Chem. Asian J.* **2011**, *6*, 1706-1727.
32. Chi, Y.; Chou, P.T. Transition-Metal Phosphors with Cyclometalating Ligands: Fundamentals and Applications. *Chem. Soc. Rev.* **2010**, *39*, 638-655.
33. King, K.A.; Spellane, P.J.; Watts, R.J. Excited State Properties of a Triply Ortho-Metalated Iridium(III) Complex. *J. Am. Chem. Soc.* **1985**, *107*, 1431-1432.
34. Sajoto, T.; Djurovich, P.I.; Tamayo, A.B.; Oxgaard, J.; Goddard, W.A.; Thompson, M.E. Temperature Dependence of Blue Phosphorescent Cyclometalated Ir(III) Complexes. *J. Am. Chem. Soc.* **2009**, *131*, 9812-9822.
35. Brooks, J.; Babayan, Y.; Lamansky, S.; Djurovich, P.I.; Tsyba, I.; Bau, R.; Thompson, M.E. Synthesis and Characterization of Phosphorescent Cyclometalated Platinum Complexes. *Inorg. Chem.* **2002**, *41*, 3055-3066.
36. Hofbeck, T.; Yersin, H. The Triplet State of *fac*-Ir(ppy)$_3$. *Inorg. Chem.* **2010**, *49*, 9290-9299.
37 Hay, P. J. Theoretical Studies of the Ground and Excited Electronic States in Cyclometalated Phenylpyridine Ir(III) Complexes Using Density Functional Theory. *J. Phys. Chem. A.* **2002**, *106*, 1634-1641.
38. Sotoyama, W.; Satoh, T.; Sato, H.; Matsuura, A.; Sawatari, N. Excited States of Phosphorescent Platinum(II) Complexes Containing N^C^N-Coordinating Tridentate Ligands: Spectroscopic Investigations and Time-Dependent Density Functional Theory Calculations. *J. Phys. Chem. A*, **2005**, *109*, 9760-9766.
39. Rochester, D.L.; Develay, S.; Zalis, S.; Williams, J.A.G. Localised to Intraligand Charge-Transfer States in Cyclometalated Platinum Complexes: An Experimental and Theoretical Study into the Influence of Electron-Rich Pendants and Modulation of Excited States by Ion Binding. *Dalton Trans.* **2009**, 1728-1741.
40. Tong, G.S.M.; Che, C.M. Emissive or Nonemissive? A Theoretical Analysis of the Phosphorescence Efficiencies of Cyclometalated Platinum(II) Complexes. *Chem. Eur. J.* **2009**, *15*, 7225-7237.
41. Lamansky, S.; Djurovich, P.; Murphy, D.; Abdel-Razzaq, F.; Lee, H. E.; Adachi, C.; Burrows, P. E.; Forrest, S. R; Thompson, M.E. Highly Phosphorescent Bis-Cyclometalated Iridium Complexes: Synthesis, Photophysical Characterization, and Use in Organic Light Emitting Diodes. *J. Am. Chem. Soc.* **2001**, *123*, 4304-4312.

42. Tsuboyama, A.; Iwawaki, H.; Furugori, M.; Mukaide, T.; Kamatani, J.; Igawa, S.; Moriyama, T.; Miura, S.; Takiguchi, T.; Okada, S.; Hoshini, M.; Ueno, K. Homoleptic Cyclometalated Iridium Complexes with Highly Efficient Red Phosphorescence and Application to Organic Light-Emitting Diode. *J. Am. Chem. Soc.* **2003**, *125*, 12971-12979.
43. Su, Y. J.; Huang, H. L.; Li, C. L.; Chien, C. H.; Tao, Y. T.; Chou, P.T.; Datta, S.; Liu, R. S. Highly Efficient Red Electrophosphorescent Devices Based on Iridium Isoquinoline Complexes: Remarkable External Quantum Efficiency over a Wide Range of Current. *Adv. Mater.* **2003**, *15*, 884-888.
44. Duan, J.P.; Sun, P.P; Cheng, C.H. New Iridium Complexes as Highly Efficient Orange-Red Emitters in Organic Light-Emitting Diodes. *Adv. Mater.* **2003**, *15*, 224-228.
45. Hwang, F.M.; Chen, H. Y.; Chen, P. S.; Liu, C. S.; Chi, Y.; Shu, C.F.; Wu, F.I.; Chou, P. T.; Peng, S. M.; Lee, G. H. Iridium(III) Complexes with Orthometalated Quinoxaline Ligands: Subtle Tuning of Emission to the Saturated Red Color. *Inorg. Chem.* **2005**, *44*, 1344-1353.
46. Wilkinson, A.J.; Puschmann, H.; Howard, J.A.K.; Foster, C.E.; Williams, J.A.G. Luminescent Complexes of Iridium(III) Containing N^C^N-Coordinating Terdentate Ligands. *Inorg. Chem.* **2006**, *45*, 8685-8699.
47. Santoro, A.; Prokhorov, A.M.; Kozhevnikov, V.N.; Whitwood, A.C.; Donnio, B.; Williams, J.A.G.; Bruce, D.W. Emissive Metallomesogens Based on 2-Phenylpyridine Complexes of Iridium(III). *J. Am. Chem Soc.* **2011**, *133*, 5248-5251.
48. The use of the more commonly encountered platinum precursor salt K_2PtCl_4 in place of $PtCl_2(NCPh)_2$ gave the same final product, albeit in somewhat inferior yield.
49. Shafikov, M.Z.; Kozhevnikov, D.N.; Bodensteiner, M.; Brandly, F.; Czerwieniec, R. Modulation of Intersystem Crossing Rate by Minor Ligand Modifications in Cyclometalated Platinum(II) Complexes. *Inorg. Chem.* **2016**, *55*, 7457-7466.
50. Murphy, L.; Williams, J.A.G. Luminescent Platinum Compounds: From Molecules to OLEDs. *Top. Organomet. Chem.* **2010**, *28*, 75-111.
51. Klein, A.; Kaim, W. Axial Shielding of $5d^8$ and $5d^7$ Metal Centers in Dimesitylplatinum Complexes with Unsaturated Chelate Ligands: Spectoscopic and Spectroelectrochemical Studies of Four Different Oxidation States. *Organometallics*, **1995**, *14*, 1176-1186.
52. Williams, J.A.G.; Beeby, A.; Davies, E.S; Weinstein, J.A.; Wilson, C. An Alternative Route to Highly Luminescent Platinum(II) Complexes: Cyclometalation with N^C^N-Coordinating Dipyridylbenzene Ligands. *Inorg. Chem.* **2003**, *42*, 8609-8611.
53. Huo, S.Q.; Carroll, J.; Vezzu, D.A.K. Design, Synthesis, and Applications of Highly Phosphorescent Cyclometalated Platinum Complexes. *Asian J. Org. Chem.* **2015**, *4*, 1210-1245.
54. Caspar, J.V.; Kober, E.M.; Sullivan, B.P.; Meyer, T.J. Application of the Energy Gap Law to the Decay of Charge-Transfer Excited States. *J. Am. Chem. Soc.* **1982**, *104*, 630-632.
55. Rausch, A.F.; Murphy, L.; Williams, J.A.G.; Yersin, H. Probing the Excited State Properties of the Highly Phosphorescent Pt(dpyb)Cl Compound by High-Resolution Optical Spectroscopy. *Inorg. Chem.* **2009**, *48*, 11407-11414.
56. Rausch, A.F.; Murphy, L.; Williams, J.A.G.; Yersin, H. Improving the Performance of Pt(II) Complexes for Blue Light Emission by Enhancing the Molecular Rigidity. *Inorg. Chem.* **2012**, *51*, 312-319.

57. Vezzu, D.A.K.; Deaton, J.C.; Jones, J.S.; Bartolotti, L.; Harris, C.F.; Marchetti, A.P.; Kondakova, M.; Pike, R.D.; Huo, S. Highly Luminescent Tetradentate Bis-Cyclometalated Platinum complexes: Design, Synthesis, Structure, Photophysics, and Electroluminescence Application. *Inorg. Chem.* **2010**, *49*, 5107-5119.
58. Cheng, G.; Kui, S.C.F.; Ang, W.H.; Ko, M.Y.; Chow, P.K.; Kwong, C.L.; Kwok, C.C.; Ma, C.; Guan, X.; Low, K.H.; Su, S.J.; Che, C.M. Structurally Robust Phosphorescent [Pt(O^N^C^N)] Emitters for High Performance Organic Light-Emitting Devices with Power Efficiency up to 126 lm W^{-1} and External Quantum Efficiency over 20%. *Chem. Sci.* **2014**, *5*, 4819-4830.
59. Tyler, F.; Li, G.; Li, J. Efficient Red-Emitting Platinum Complex with Long Operational Stability. *ACS Appl. Mater. Interfaces* **2015**, *7*, 16240–16246.
60. Yersin, H.; Donges, D. Low-Lying Electronic States and Photophysical Properties of Organometallic Pd(II) and Pt(II) Compounds. Modern Research Trends Presented in Detailed Case Studies. *Top. Curr. Chem.* **2001**, *214*, 81-186.
61. Rausch, A.F.; Homeier, H.H.H.; Djurovich, P.I.; Thompson, M.E.; Yersin, H. Spin-Orbit Coupling Routes and OLED Performance – Studies of Blue-Light Emitting Ir(III) and Pt(II) Complexes. *Proc. SPIE* **2007**, 6655.
62. Rausch, A.F.; Homeier, H.H.H.; Yersin, H. Organometallic Pt(II) and Ir(III) Triplet Emitters for OLED Applications and the Role of Spin-Orbit Coupling: A Study Based on High-Resolution Optical Spectroscopy. *Top. Organomet. Chem.* **2010**, *29*, 193-235.
63. Fischer, T.; Czerwieniec, R.; Hofbeck, T.; Osminina, M.M.; Yersin, H. Triplet State Properties of a Red Light-Emitting [Pt(s-thpy)(acac)] Compound. *Chem. Phys. Lett.* **2010**, *486*, 53-59.
64. M. J. Frisch, G. W. Trucks, H. B. Schlegel, G. E. Scuseria, M. A. Robb, J. R. Cheeseman, G. Scalmani, V. Barone, B. Mennucci, G. A. Petersson, H. Nakatsuji, M. Caricato, X. Li, H. P. Hratchian, A. F. Izmaylov, J. Bloino, G. Zheng, J. L. Sonnenberg, M. Hada, M. Ehara, K. Toyota, R. Fukuda, J. Hasegawa, M. Ishida, T. Nakajima, Y. Honda, O. Kitao, H. Nakai, T. Vreven, Jr., J. A. Montgomery, J. E. Peralta, F. Ogliaro, M. Bearpark, J. J. Heyd, E. Brothers, K. N. Kudin, V. N. Staroverov, R. Kobayashi, J. Normand, K. Raghavachari, A. Rendell, J. C. Burant, S. S. Iyengar, J. Tomasi, M. Cossi, N. Rega, J. M. Millam, M. Klene, J. E. Knox, J. B. Cross, V. Bakken, C. Adamo, J. Jaramillo, R. Gomperts, R. E. Stratmann, O. Yazyev, A. J. Austin, R. Cammi, C. Pomelli, J. W. Ochterski, R. L. Martin, K. Morokuma, V. G. Zakrzewski, G. A. Voth, P. Salvador, J. J. Dannenberg, S. Dapprich, A. D. Daniels, O. Farkas, J. B. Foresman, J. V. Ortiz, J. Cioslowski, D. J. Fox, *Gaussian 09*, Revision A.02, Gaussian, Inc., Wallingford CT, 2009.
65. Pashazadeh, R.; Pander, P.; Lazauskas, Dias, F.B.; Grazulevicius, J.V. Multicolor Luminescence Switching and Controllable Thermally Activated Delayed Fluorescence Turn On / Turn Off in Carbazole-Quinoxaline-Carbazole Triads. *J. Phys. Chem. Lett.* **2018**, *9*, 1172-1177.
66. Cook, J.H.; Al-Attar, H.; Monkman, A.P. Effect of PEDOT-PSS Resistivity and Work Function on PLED Performance. *Org. Electron.* **2014**, *15*, 245-250.
67. Kim, D. H.; Cho, N. S.; Oh, H. Y.; Yang, J. H.; Jeon, W. S.; Park, J. S.; Suh, M. C.; Kwon, J. H. Highly Efficient Red Phosphorescent Dopants in Organic Light-Emitting Devices. *Adv. Mater.* **2011**, *23*, 2721-2726.
68. Fan, C.-H.; Sun, P.; Su, T.H.; Cheng, C.H. Host and Dopant Materials for Idealised Deep-Red Organic Electrophosphorescence Devices. *Adv. Mater.* **2011**, *23*, 2981-2985.

69. Li, G.; Li, P.; Zhuang, X.; Ye, K.; Liu, Y.; Wang, Y. Rational Design and Characterization of Heterolpetic Phosphorescent Complexes for Highly Efficient Deep-Red Organic Light-Emitting Devices. *ACS Appl. Mater. Interfaces* **2017**, *9*, 11749-11758.
70. Jou, J.H.; Su, Y.T.; Hsiao, M.T.; Yu, H.H.; He, Z.K.; Fu, S.C.; Chaing, C.H.; Chen, C.T.; Chou, C.H.; Shyue, J.J. Solution-Process-Feasible Deep-Red Phosphorescent Emitter. *J. Phys. Chem. C*, **2016**, *120*, 18794-18802.
71. Liu, X.; Yao, B.; Zhang, Z.; Zhao, X.; Zhang, B.; Wong, W.Y.; Cheng, Y.; Xie, Z. Power-Efficient Solution-Processed Red Organic Light-Emitting Diodes Based on an Exciplex Host and a Novel Phosphorescent Iridium Complex. *J. Mater. Chem. C.*, **2016**, *4*, 5787-5794.
72. Bezvikonnyi, O.; Gudeika, D.; Volyniuk, D.; Grazulevicius, J.V.; Bagdziunas, G. Pyrenyl Substituted 1,8-Naphthalimide as a New Material for Weak Efficiency-Roll-Off Red OLEDs: A Theoretical and Experimental Study. *New J. Chem.* **2018**, *42*, 12492-12502.
73. Ly, K.T.; Chen-Cheng, R.W.; Lin, H.-W.; Shiau, Y.-J.; Liu, S.-H.; Chou, P.-T.; Tsao, C.-S; Huang, Y.-C.; Chi, Y. Near-Infrared Organic Light-Emitting Diodes with Very High External Quantum Efficiency and Radiance. *Nat. Photonics* **2017**, *11*, 63-68.
74. Yang, X.; Jiao, B.; Sun, Y.; Wu, Y.; Zhou, G.; Wong, W.-Y. Achieving High-Performance Solution-Processed Orange OLEDs with the Phosphorescent Cyclometalated Trinuclear Pt(II) Complex. *ACS Appl. Mater. Interfaces* **2018**, *10*, 10227-10235.
75. Cebrián, C.; Mauro, M.; Kourkoulos, D.; Mercandelli, P.; Hertel, D.; Meerholz, K.; Strassert, C. A.; De Cola, L. Luminescent Neutral Platinum Complexes Bearing an Asymmetric N^N^N Ligand for High-Performance Solution-Processed OLEDs. *Adv. Mater.* **2013**, *25*, 437-442.
76. Mróz, W.; Botta, C.; Giovanella, U.; Rossi, E.; Colombo, A.; Dragonetti, C.; Roberto, D.; Ugo, R.; Valore, A.; Williams, J. A. G. Cyclometallated Platinum(II) Complexes of 1,3-Di(2-pyridyl)benzenes for Solution-processible WOLEDs Exploiting Monomer and Excimer Phosphorescence. *J. Mater. Chem.* **2011**, *21*, 8653-8661.
77. Cardona, C.M.; Li, W.; Kaifer, A.E.; Stockdale, D.; Bazan, G.C. Electrochemical Considerations for Determining Absolute Frontier Orbital Energy Levels of Conjugated Polymers for Solar Cell Applications. *Adv. Mater.* **2011**, *23*, 2367-2371.

Graphic for Table of Contents Entry